International Journal of Solids and Structures 000 (2018) 1–11

Contents lists available at ScienceDirect

International Journal of Solids and Structures

journal homepage: www.elsevier.com/locate/ijsolstr

Aging-dependent strain localization in amorphous glassy polymers: From necking to shear banding

Run Zhang[1], Pengxiang Bai[1], Dong Lei, Rui Xiao*

Department of Engineering Mechanics, College of Mechanics and Materials, Hohai University, Nanjing, Jiangsu 210098, China

ARTICLE INFO

Article history:
Received 7 November 2017
Revised 14 March 2018
Available online xxx

Keywords:
Shear banding
Necking
Physical aging
PETG
DIC

ABSTRACT

This study investigates the influence of physical aging on the tensile deformation behaviors of poly(ethylene terephthalate)-glycol. The polymers are subjected to a quenched and an annealed heat treatment, followed by deformation in tension. The digital image correlation (DIC) is used to capture the surface strain. The DIC results show that the deformation localization occurs in the post-yield strain softening region. The quenched and annealed polymers exhibit different localization types, representing as necking for quenched polymers and shear banding for annealed polymers. With the help of the DIC, the nucleation and propagation of the localization zones are fully captured. The DIC results show that the reference location with the maximum strain does not change with the deformation. At the same strain level, the maximum strain in the shear bands is much larger than that in the necks, which explains the failure strain of the annealed polymers is smaller than the quenched polymers. The stretch rate also has a strong effect on the localization behaviors. A larger stretch rate results in a stronger localization due to an increase in the amount of strain softening.

1. Introduction

Deformation localization, such as crazing (Legrand, 1969; Argon, 2011; Jiang et al., 2017), necking (Neale and Tugcu, 1985; Wu and van der Giessen, 1995; Li and Buckley, 2009) and shear banding (Brady and Yeh, 1971; Wu and Turner, 1973; Chau and Li, 1979), can result in an early failure of polymers, which significantly limits the applications of polymers as load-bearing materials. While crazing occurs in the pre-yield region, the necking and shear banding appear in the post-yield region. The post-yield strain softening in polymers is the intrinsic reason for the occurring of necking and shear banding (Govaert et al., 2000; Li and Buckley, 2010), which allows the coexistence of zones with different strain. The glassy polymers exhibit strain hardening at large deformation. Thus, the deformation localization zone propagates after initializing, which is different from the localization behaviors in metals (Wu and van der Giessen, 1994; 1995).

The nature of the deformation localization depends on temperature, loading rate, physical aging and mechanical deformation (Legrand, 1969; Dooling et al., 2002; Stoclet et al., 2014; van Melick et al., 2003; Govaert et al., 2000; Archer and Lesser, 2011; Dobovšek and Polonica, 2015). Jang et al. (1984) demonstrated that ductile failure changed to crazing-induced brittle failure when decreasing temperatures and increasing strain rates for a variety of polymers. Dooling et al. (2002) showed that a transition from homogeneous deformation to necking in poly (methyl methacrylate) can occur when deformed above a critical strain rate or below a critical temperature. Temperature and strain rate also influence the morphology of shear bands. Coarse bands often appear at low temperatures and high rates, while fine bands can be observed at high temperatures and low rates (Dobovšek and Polonica, 2015). Physical aging can induce a more severe localization behavior, while mechanical pre-deformation can reverse the effects of physical aging. Yang et al. (1996) found that a homogeneous deformation was observed for the quenched poly (phenylene oxide), which changed to necking as aging and a brittle failure for the heavily aged condition. Deformation localization in some polymers can be eliminated by pre-deformation such as cold rolling (van Melick et al., 2003) and drawing (Unwin et al., 2002). Several excellent reviews are also available for localization behaviors in polymers. Tomita et al. (1998) provided a full discussion on the onset of necking, the propagation of necked region, the temperature change and the transition of necking to shear banding with predrawing. Meijer and Govaert (2005) reviewed the influence of the nonequilibrium structure on the localization behaviors of amorphous polymers.

* Corresponding author.
E-mail address: rxiao@hhu.edu.cn (R. Xiao).
[1] These authors contribute equally to this work.

https://doi.org/10.1016/j.ijsolstr.2018.03.030
0020-7683/

Based on the constitutive theories of glassy polymers (Boyce et al., 1992; Wu and Van der Giessen, 1996; Tomita et al., 1997; Tomita, 2000; Chowdhury et al., 2008; Li and Buckley, 2010; Xu et al., 2017; Kweon and Benzerga, 2013), the intrinsic strain softening plays a fundamental role on the deformation localization behaviors. Physical aging, also named as structural relaxation, determines the amount of strain softening (Xiao and Nguyen, 2015; Xiao et al., 2017). When approaching the glass transition temperature, the polymer structure falls out of the equilibrium. This nonequilibrium state continuously evolves towards an equilibrium state. This aging process can result in a more sluggish polymer structure, accompaned with a decrease in volume, enthalpy and an increase in viscosity, yield strength (Xiao et al., 2013; Liu et al., 2015). The mechanical deformation can induce an opposite effect on the polymer structure compared with physical aging, driving the polymer structure away from the equilibrium state, a process known as mechanical rejuvenation (Kierkels et al., 2008; Semkiv and Hütter, 2016). The amount of stress softening increases with aging and decreases with mechanical pre-deformation, which explains the effects of the physical aging and mechanical pre-deformation on the localization behaviors (Cross and Haward, 1978; Govaert et al., 2000).

The traditional experimental methods, such as strain gauge, can not capture the full field deformation behaviors. Also, those methods can only measure the small strain behaviors. The recent development of the non-contacted optical experimental techniques, such as digital image correlation (DIC), has provided a powerful tool to investigate the inhomogeneous deformation of various materials, such as biomaterials (Murienne et al., 2016), concrete (Lei et al., 2017), metals (Cai et al., 2016; Tung et al., 2010; Gao et al., 2015; Pan et al., 2015) and polymers (Grytten et al., 2009; Jerabek et al., 2010). Yu et al. (2016) applied DIC to study the necking of aluminum alloys. Zhu et al. (2012) used DIC to investigate the shear band nucleation and broadening in the nanocrystalline Ni sheet. Pan et al. (2016) applied high speed stereo-DIC to describe the deformation of an aluminum panel under impact. Compared with metals, the deformation of polymers typically involves with large deformation. Heinz and Wiggins (2010) applied the DIC to characterize the strain distribution during compression and found homogeneous deformation can only be observed in the pre-yield region. Ye et al. (2015) demonstrated that 3D DIC can fully capture the necking behaviors of high-density polyethylene up to a true strain 1.8. Poulain et al. (2013) and Engqvist et al. (2014) compared the performance of the DIC and other techniques to measure the localization behaviors of polymers at large deformation and found the DIC was more reliable. Pan et al. (2009) reviewed the methodologies of the DIC technique and the accuracy of strain estimation using DIC.

In this work, we will utilize the DIC to investigate the influence of physical aging on the strain localization behaviors of poly(ethylene terephthalate)-glycol (PETG). PETG is an amorphous copolymer of poly(ethylene terephthalate) (PET). However, it has not been as widely used as PET in industrial areas mainly due to the fact that PETG does not show stretch-induced crystallization as PET does. Recent works have shown that PETG has its own advantages, such as transparent, easy processing, high toughness and excellent mechanical properties (Kattan et al., 2001; Dupaix and Boyce, 2005). This investigation can further enrich our understanding of PETG and potentially promote the applications of PETG.

The paper is arranged as follows. The experimental procedures are shown in Section 2. Section 3 presents the deformation localization behaviors of the quenched and annealed polymers, followed by a discussion regarding the obtained results. The conclusion part summarizes the main findings and the future directions.

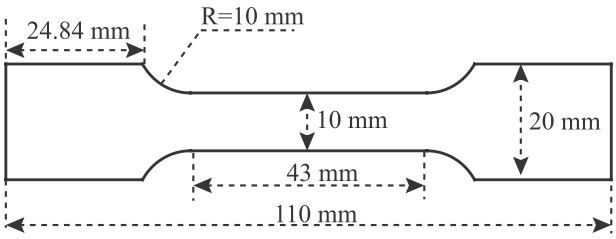

Fig. 1. The geometry of the specimens used in uniaxial tension tests.

2. Experimental methods

The PETG film with 1.59 mm (1/16 inch) thickness was obtained from McMaster-Carr Supply Company. The film was used in as-received conditions and was laser cut to the specific experimental geometry before testing.

2.1. Differential scanning calorimetry and dynamic temperature sweep tests

The differential scanning calorimetry (DSC) was used to characterize the phase transition behaviors of the obtained PETG, while the dynamic mechanical analysis (DMA) was used to describe the glass transiton behaviors. Square specimen weighting 10 mg was cut form the PETG film and placed in a differential scanning calorimeter TA Q20 (TA Instruments, New Castle, DE). The specimen was heated from 25 °C to 110 °C at 5 °C/min.

To measure the dynamic modulus, film specimen with size 15 mm × 5 mm × 1.59 mm was used. The test was run on a dynamic mechanical analyzer TA Q800 (TA Instruments, New Castle, DE). The as-received specimen subject to a 0.2% dynamic strain in the tension mode was heated from 20 °C to 130 °C at 2 °C/min. The frequency of the dynamic test was chosen as 1 Hz.

2.2. Uniaxial tension tests

The geometry of tensile specimens is shown in Fig. 1. Before the thermal treatment, the specimens were sprayed with random speckles. To remove the effects of previous thermal history, the specimens were first equilibrated at 110 °C for 30 min in a thermal chamber. The quenched specimens were obtained through transferring the specimens from the thermal chamber to water at room temperature. For the annealed condition, the temperature of the thermal chamber was decreased step-wise by 10 °C each time and held for 30 min until room temperature. The total process took 4 to 5 h. The size of the specimen showed no change after thermal treatment, which indicated no molecular orientation existed in as-received materials. The uniaxial tension tests were performed on the quenched and annealed specimens using Electronic Universal Material Testing Machine Instron 3360 Series Testing Machine at room temperature (20–24 °C) with a 30 kN load cell . Three loading rates were chosen: 0.774 mm/min, 7.74 mm/min and 77.4 mm/min. During the tension tests, a high precision CCD camera with the M0814-MP's megapixel lens of Japan Computer was used to record the surface of the specimens. The resolution of each image was 1624 × 1224 pixels^2. In our setup, one pixel represents 0.04 mm. The strain resolution of this DIC system is 0.01%.

3. Results

The DSC result in Fig. 2-a shows that the PETG exhibits a glass transition behavior. No endothermic peak was observed during the heating process. This indicates that no melting transition has been observed until 110°C. This is consistent with the observations in Kattan et al. (2001). PETG tends to resist crystallization,

Please cite this article as: R. Zhang et al., Aging-dependent strain localization in amorphous glassy polymers: From necking to shear banding, International Journal of Solids and Structures (2018), https://doi.org/10.1016/j.ijsolstr.2018.03.030

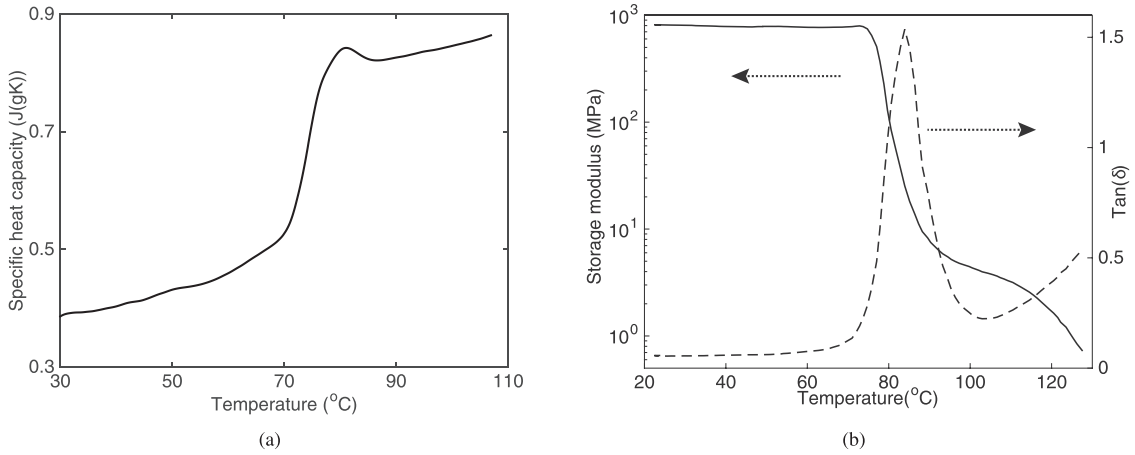

(a) (b)

Fig. 2. (a) The specific heat capacity of PETG as a function of temperature measured by DSC at a heating rate of 5 °C/min, and (b) storage modulus and tan δ of PETG as a function of temperature for a dynamic tensile test at a frequency of 1 Hz and heating rate of 2 °C/min.

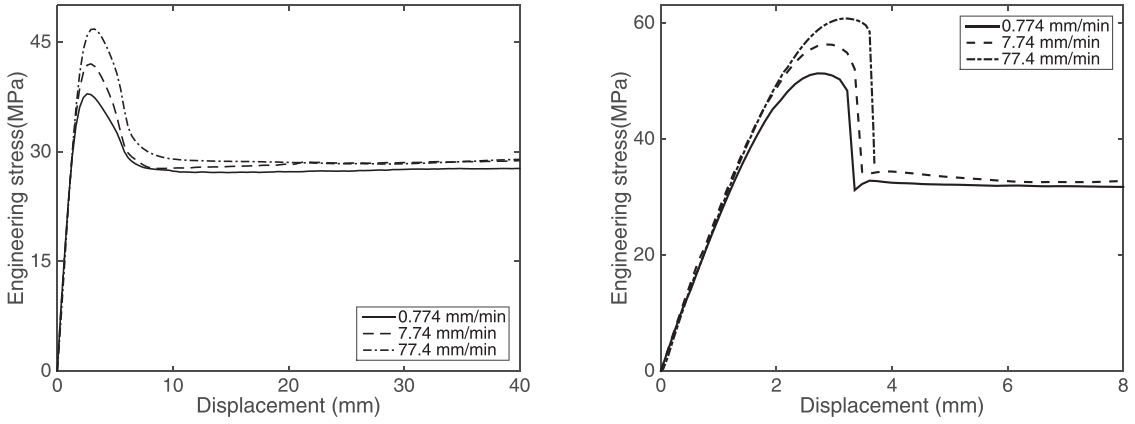

(a) (b)

Fig. 3. The stress response of (a) quenched specimens, and (b) annealed specimens deformed at different stretch rates.

though crystallization can occur during high temperature stretching. We also used the dynamic temperature sweep test to characterize the glass transition behavior of PETG. As shown in Fig. 2-b, the glass transition region of PETG spanned from 75 °C to 100 °C with the maximum tan δ occurring at 84 °C. The polymers did not exhibit an equilibrium rubbery plateau. The modulus continuously decreased as the temperature increased, which indicated that the PETG was a reprocessable amorphous thermoplastic. The glass transition region obtained from DSC and DMA is consistent.

The stress response of the quenched and annealed specimens is shown in Fig. 3. The engineering stress was calculated through dividing the force by the original cross section area, while the displacement in this figure and all the following figures represents the displacement of the machine grips. The PETG exhibited an extremely ductile behavior in the quenched conditions. The failure displacement at the two lower stretch rates was more than 200% of the gauge length. The yield strength increased with the stretch rate while the steady state flow stress only slightly depended on the stretch rate. No apparent strain hardening behaviors were observed. This was because the engineering stress rather than the true stress was plotted. Due to the inhomogeneous deformation, the true stress and true strain also vary with the location of specimens. The experimental results of Dupaix and Boyce (2005) and our preliminary study showed that in the uniaxial compression tests, the PETG exhibited a homogeneous deformation and a clear strain hardening behavior can be observed at large strain. Physical aging has a strong effect on the strain softening behaviors. The annealed polymers exhibited a much larger strain softening than quenched specimens. The amount of strain softening also in-

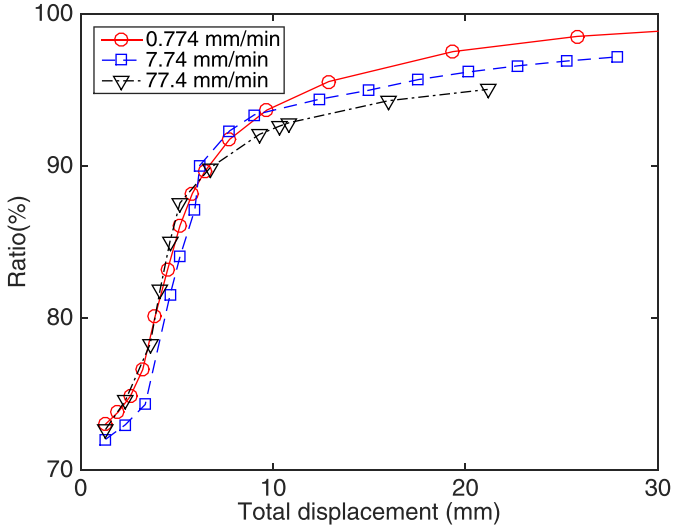

Fig. 4. The ratio between the displacement of the parallel-sided central section and the grip as a function of the total displacement for quenched polymers at various stretch rates. .

Please cite this article as: R. Zhang et al., Aging-dependent strain localization in amorphous glassy polymers: From necking to shear banding, International Journal of Solids and Structures (2018), https://doi.org/10.1016/j.ijsolstr.2018.03.030

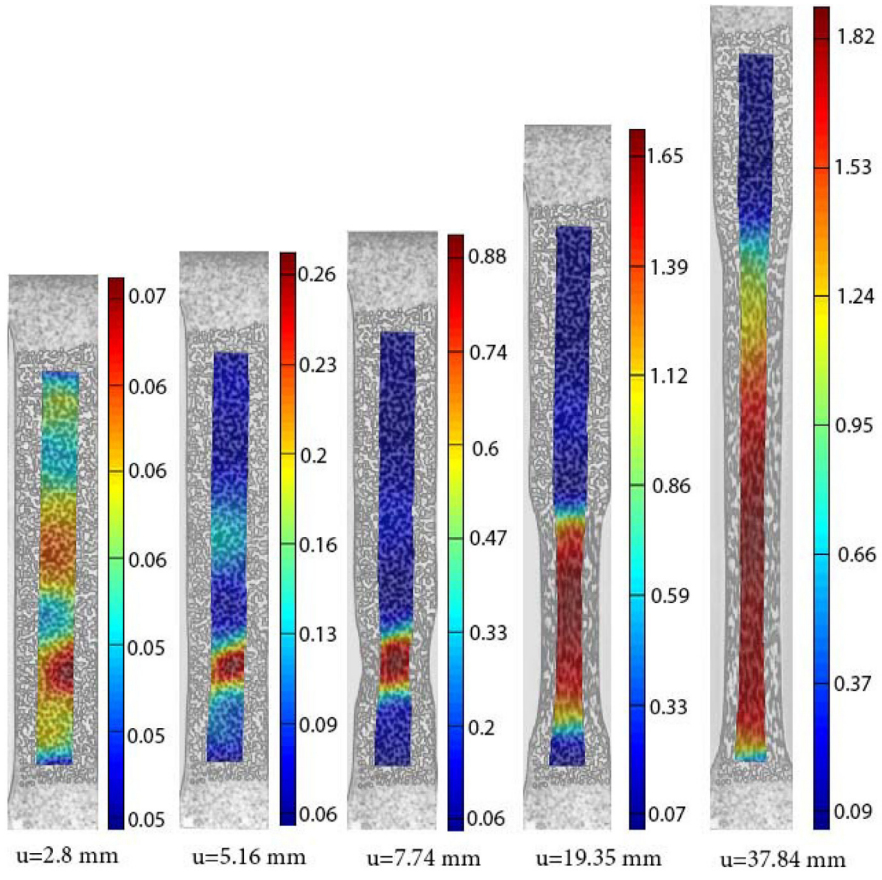

(a)

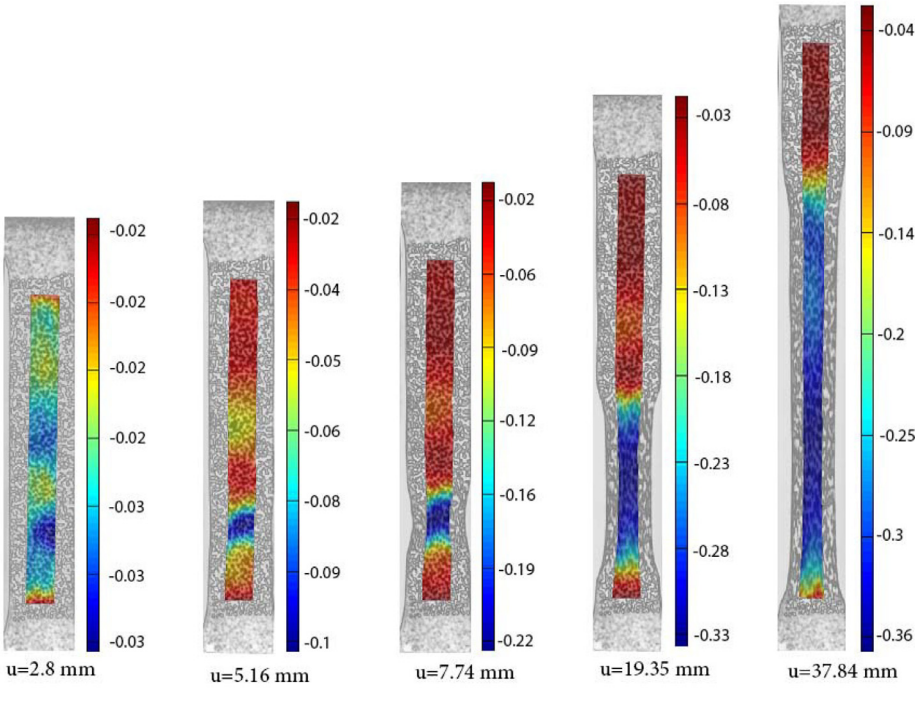

(b)

Fig. 5. Strain contours of a) ϵ_{yy} and b) ϵ_{xx} for quenched polymers at stretch rate of 0.774 mm/min.

Please cite this article as: R. Zhang et al., Aging-dependent strain localization in amorphous glassy polymers: From necking to shear banding, International Journal of Solids and Structures (2018), https://doi.org/10.1016/j.ijsolstr.2018.03.030

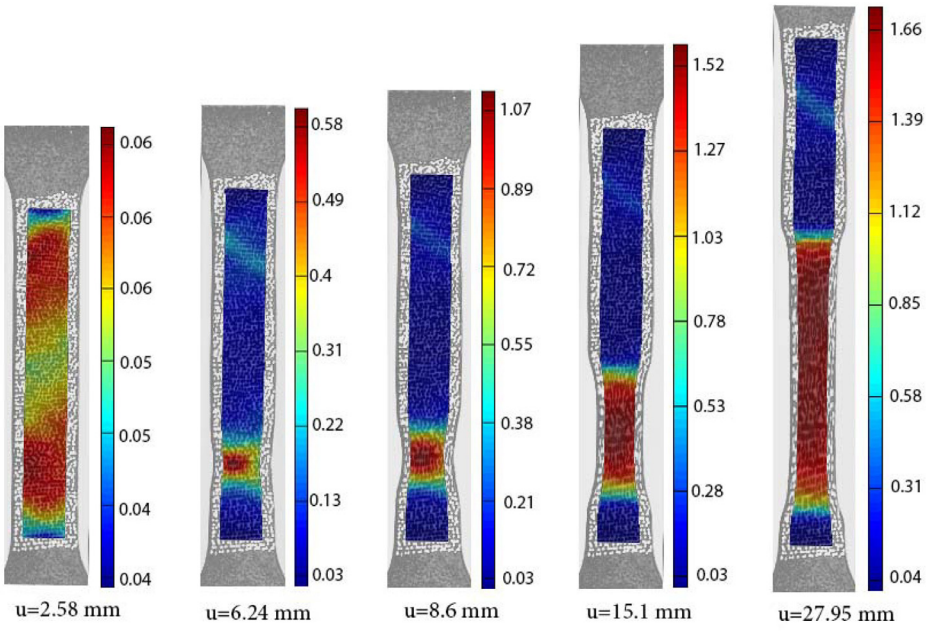

(a)

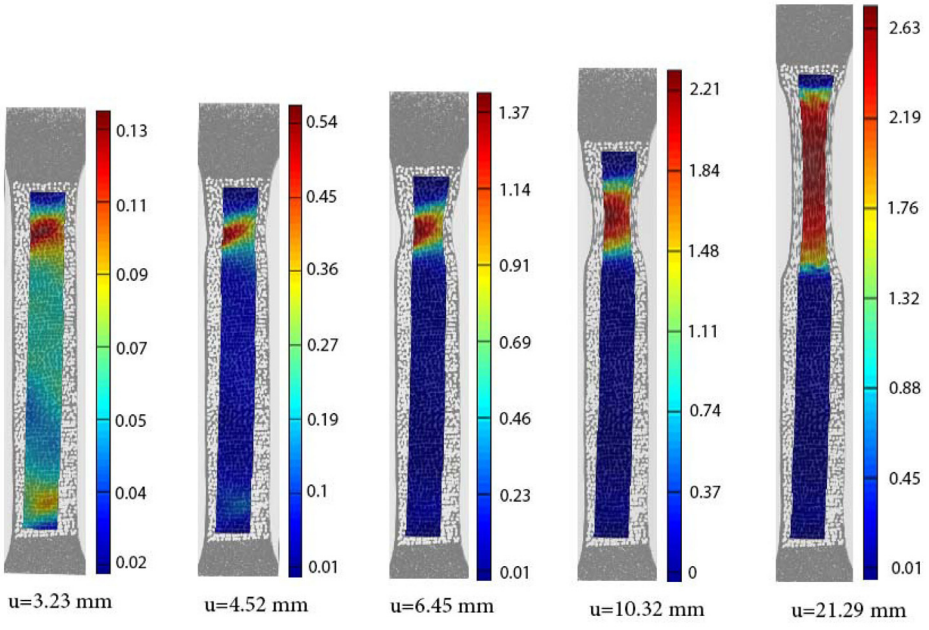

(b)

Fig. 6. Strain contours of ϵ_{yy} for quenched polymers at stretch rate of a) 7.74 mm/min and b) 77.4 mm/min.

creased with the strain rate for annealed polymers. Thus, the maximum amount strain softening (around 28 MPa) occurred for annealed specimens at the stretch rate of 77.4 mm/min, while the stress only decreased around 8 MPa for quenched specimens at the stretch rate of 0.774 mm/min. The annealed polymers also exhibited a much sharper softening behavior than the quenched polymers. The steady state flow stress was reached at around displacement of 6.5 mm for the quenched polymers while this value was less than 4 mm for the annealed polymers. The steady state flow stress of annealed specimens was around 4 MPa higher than that of the quenched specimens. This was different to the observations in the uniaxial compression tests, where the steady state flow stress was independent on the thermal history (Xiao and Nguyen, 2015). One possible reason was that different localization types were observed for the quenched and annealed conditions, which may influence the steady state flow stress.

The authors want to emphasize in the experiments the displacement of the machine grips is controlled, which is not the same as the displacement of the parallel-sided central section. However, from the DIC, the displacement of the central gauge section can be obtained. As shown in Fig. 4, the ratio between the displacement of parallel-sided central section and machine grips is plotted as a function of the total displacement. The results showed that this ratio was between 0.7 and 0.8 in the pre-yield region.

Please cite this article as: R. Zhang et al., Aging-dependent strain localization in amorphous glassy polymers: From necking to shear banding, International Journal of Solids and Structures (2018), https://doi.org/10.1016/j.ijsolstr.2018.03.030

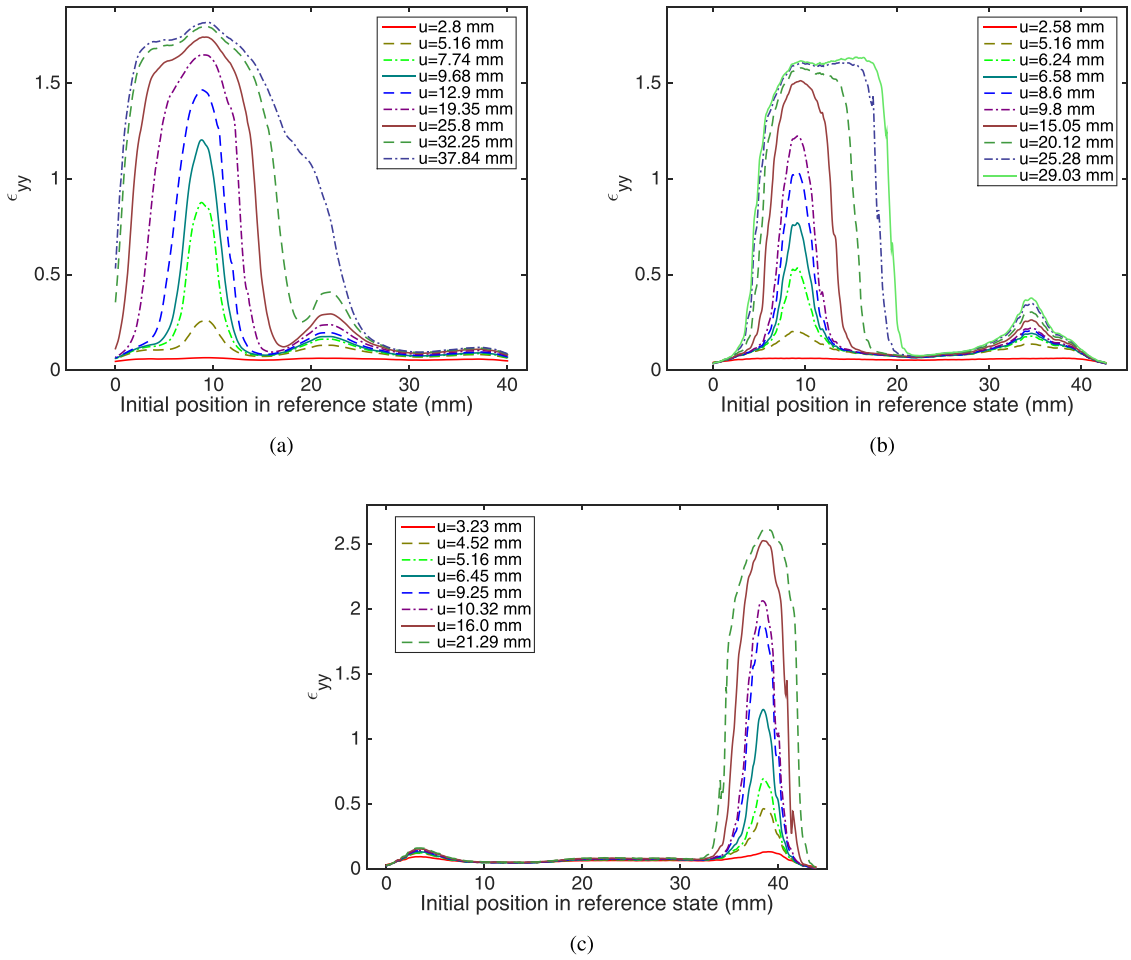

Fig. 7. Section line plots of ϵ_{yy} to show the evolution of the necks at stretch rate of a) 0.774 mm/min, b) 7.74 mm/min and c) 77.4 mm/min.

When the localization began to form, the corresponding engineering strain rate was obtained as following: 2.4×10^{-4}/s for stretch rate of 0.774 mm/min, 2.3×10^{-3}/s for stretch rate of 7.74 mm/min and 2.3×10^{-2}/s for stretch rate of 77.4 mm/min. It was also found the ratio gradually increased to nearly 100% with the deformation. The total increase of the displacement in the central section was close to the displacement of the grips in the post-yield region. This was reasonable since the other parts remained in the pre-yield region and the deformation only slightly changed. Thus, when the localization zone began to propagate, the engineering strain rate can be approximated as the ratio between stretch rate and the gauge length (43 mm). For annealed polymers, the results are the same. The stretch direction was defined as the y direction and the horizontal direction along the surface of the specimen was defined as the x direction. Fig. 5 plots the contours of engineering strain ϵ_{yy} and ϵ_{xx} of the quenched specimens deformed at stretch rate of 0.774 mm/min. The engineering strain is calculated as $\epsilon_{xx} = \frac{\partial u}{\partial X}$ and $\epsilon_{yy} = \frac{\partial v}{\partial Y}$, where u and v are the displacement in the x and y directions, X and Y are initial positions. In the pre-yield region, the specimens exhibited a nearly homogeneous deformation with the maximum and minimum strain varying within 0.01. When approaching the yield point, inhomogeneous deformation appeared. As shown in the first snapshot of Fig. 5, zones with higher strain can be observed in the middle and lower parts of specimens, while a slightly severe localization occurred at the lower part. The localization in these two zones continued to nucleate. When the displacement reached 5.16 mm, a clear localization zone can be observed in the lower part. The strain in this small region was 4 times of the minimum strain in the specimen. In comparison, the localization zone in the middle part was not as clear. At this stage, necking can not be seen by the naked eyes. With further deformation, a neck showed in the lower part. The strain in the neck was much larger than the remaining part. The neck continuously propagated along the whole specimen. The contours also showed that the strain out of the localization zone was small during all the deformation process. Since we used 2D DIC, the strain in the thickness direction was not calculated. As a consequence, the information regarding the volumetric deformation can not be obtained. Also whether the deformation in the thickness and width direction is isotropic remains an unsolved question.

The contours of ϵ_{yy} for quenched specimens at stretch rate of 7.74 mm/min and 77.4 mm/min are shown in Fig. 6. The phenomena were close to the observations of the specimen deformed at stretch rate of 0.774 mm/min. For the specimen deformed at 7.74 mm/min, in addition to the neck in the lower part, an inclined narrow region with strain localization can be observed in the upper part of the specimen. This looked like a shear band, since the localization zone has an inclination to the deformation axis. The angle between the "band" and the stretching direction was 58°, which was close to the theoretical prediction 55° of shear banding (Thomas, 1953). However, the strain in this localization zone was much smaller compared to shear bands of the annealed polymers reported in the latter part of the paper. The neck of the specimen deformed at 77.4 mm/min was more pronounced than the specimens deformed at the other two stretch rates. This was because a larger stretch rate can cause a larger strain softening. This was con-

Please cite this article as: R. Zhang et al., Aging-dependent strain localization in amorphous glassy polymers: From necking to shear banding, International Journal of Solids and Structures (2018), https://doi.org/10.1016/j.ijsolstr.2018.03.030

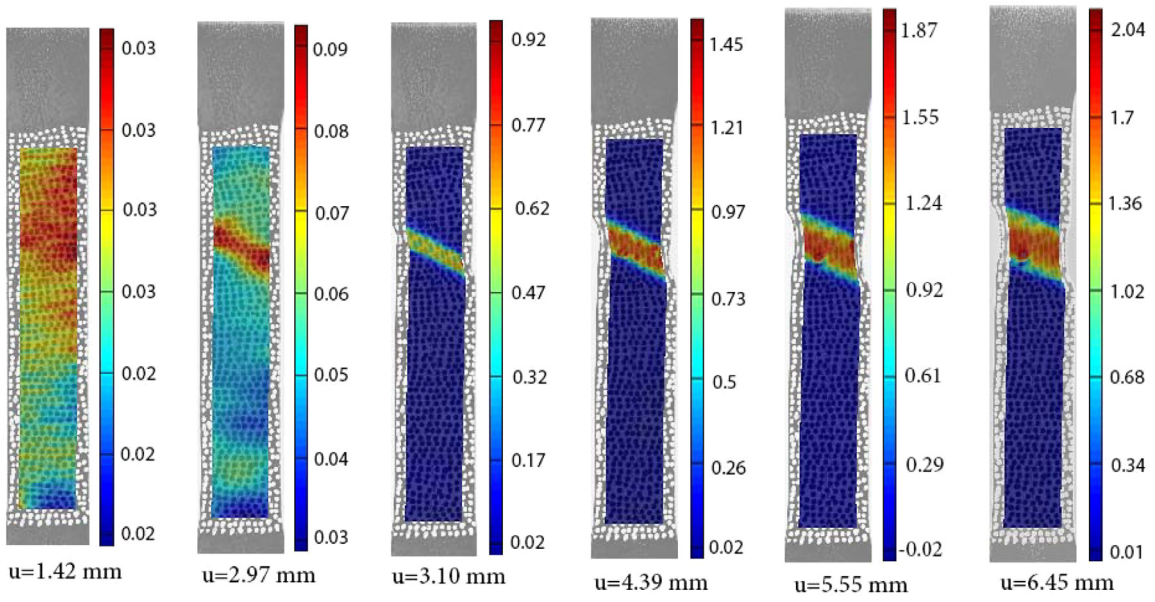

(a)

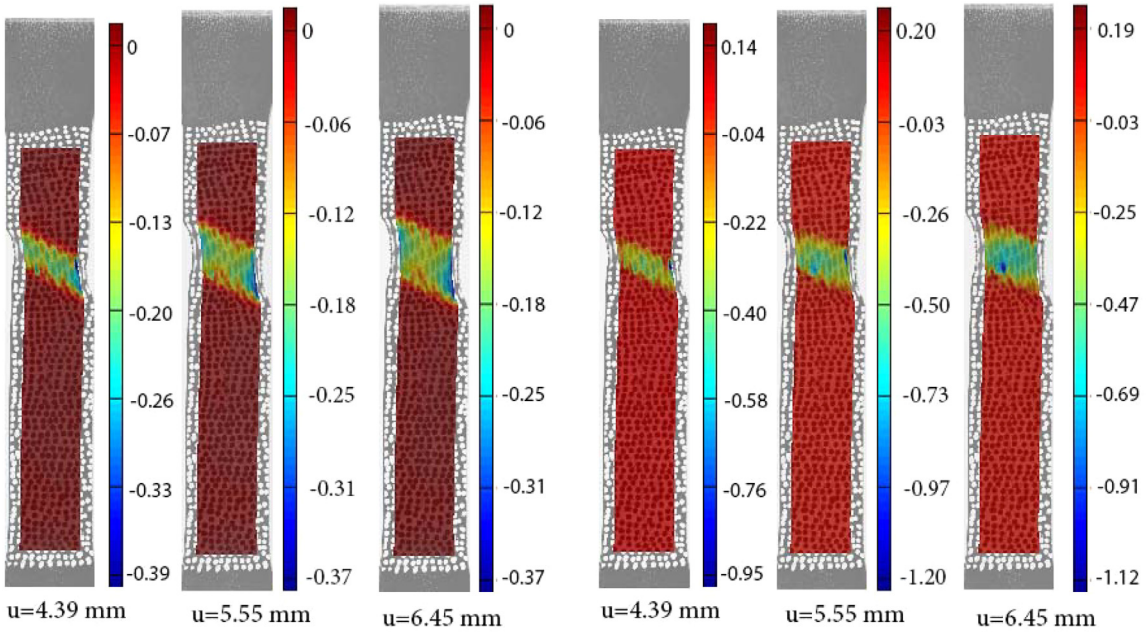

(b) (c)

Fig. 8. Strain contours of a) ϵ_{yy}, b) ϵ_{xx} and c) γ_{xy} for annealed polymers at stretch rate of 0.774 mm/min.

sistent with the simulation results (Li and Buckley, 2009) and the experimental results (Ye et al., 2015). We also noticed that the location of the neck occurred randomly in the tensile tests. This was because the gauge length of the specimens chosen was relatively large. The localization initiated at the weakest point of the specimen. This was different from the necking behaviors of specimens with a small gauge, where the localization typically occurred in the middle of the specimens. We only plotted the contours to a certain strain because the DIC software failed to calculate the strain at the highly deformed regions.

To quantitatively demonstrate the formation and propagation of the necks, we plot the strain along the vertical line in the middle of the specimen in Fig. 7. These data provided more detailed information regarding the formation and development of the neck. In all three conditions, necks first formed at a specific location. The maximum strain always occurred in this reference position and did not change with deformation. The shape of the strain profile at the early stage had a sharp peak, which showed a large strain gradient within the neck. The necks propagated in both directions. At the large deformation, a plateau region of the strain profile was formed. This indicated that a nearly homogeneous deformation was achieved in the necks. Interestingly, in addition to the main localization zone, a smaller and less pronounced localization region can always be observed regardless the stretch rate. The two regions eventually merged into one part at a large strain.

Please cite this article as: R. Zhang et al., Aging-dependent strain localization in amorphous glassy polymers: From necking to shear banding, International Journal of Solids and Structures (2018), https://doi.org/10.1016/j.ijsolstr.2018.03.030

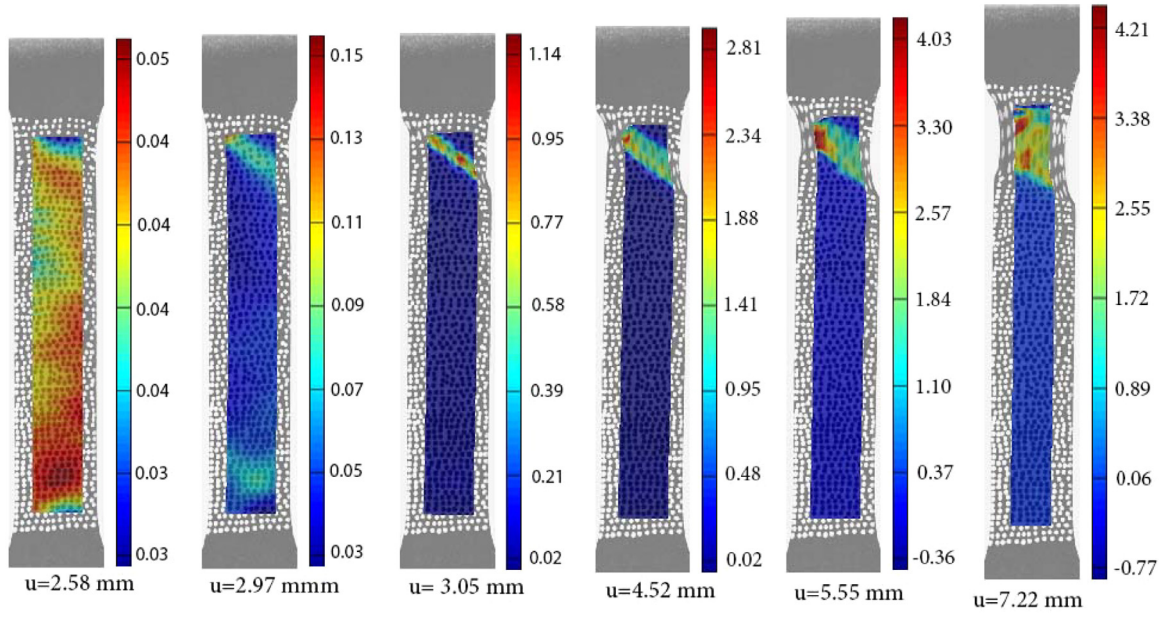

Fig. 9. Strain contours of ϵ_{yy} for annealed polymers at stretch rate of 7.74 mm/min.

The contours of ϵ_{yy} and ϵ_{xx} for annealed specimens at stretch rate of 0.774 mm/min are shown in Fig. 8-a and b. An inclined localization zone appeared when the strain reached the yield point. The strain in the zone was only slightly larger than the other parts when the displacement reached 2.97 mm. A pronounced strain localization zone representing as a shear band appeared when the displacement reached 3.10 mm. A sharp interface existed between the band and the other part of the specimen. The strain in the band was orders of magnitude larger than the strain out of the band. The band width was broadened with the deformation. At the meantime, the maximum strain in the band also increased with the deformation. Fig. 8-c plots the shear strain γ_{xy}, which was calculated based on Green–Lagrange strain. As shown, considerable shear strain existed in the localization zones. But the magnitude of the normal strain was comparable with the shear strain. This localization behavior was named as a combination of inclined neck and shear band by Bowden (1973). However, in various literatures (Bauwens, 1967; Tomita, 2000; Sweeney et al., 2007; Dobovšek and Polonica, 2015), this was also loosely named as shear band. The main feature of the shear bands observed in this work is consistent with the results in literatures for both experimental observations (Bauwens, 1967; Sweeney et al., 2007) and simulation results (Tomita, 2000; Dobovšek and Polonica, 2015). The band nucleation and propagation of the annealed polymers at stretch rate of 7.74 mm/min was similar (Fig. 9). At the same global displacement, the maximum strain in the band increased with the stretch rate. When the stretch rate was 77.4 mm/min, a shear band also appeared when reaching the yield point. However, the specimens quickly failed at the location of the shear band. No apparent shear band propagation can be observed. We also measured the initial band angle, which was defined as the angle between the shear band and the stretching direction. The band angle was 59° for stretch rate of 0.774 mm/min, 56° for stretch rate of 7.74 mm/min, and 58° for stretch rate of 77.4 mm/min. All these values were close to the theoretical prediction of 55° made by Thomas (1953).

Fig. 10 plots the strain ϵ_{yy} along the vertical middle line of the specimens. In order to see clearly the strain within the band, we also amplified the band regions in the figure. Compared with necking, shear bands occurred in a narrower region. The results clearly showed the band was broadened in both directions with the deformation. The maximum strain occurred in the middle of the band and increased with the global deformation. The detailed information about the shear bands formation and propagation can provide a useful verification result for the future models devoted to simulating shear banding.

4. Discussion

Necking in glassy polymers has been widely experimental characterized and successfully simulated by finite element models (Boyce et al., 1992; Tomita et al., 1998; Govaert et al., 2000; Li and Buckley, 2009). In order to capture the main features of necking, the constitutive models need to incorporate both the post-yield strain softening and strain hardening mechanism. To simulate strain softening, Boyce et al. (1992) adopted a phenomenological evolution equation of yield strength with viscous strain rate, while Li and Buckley (2009) used the strain-induced structural rejuvenation based on Tool's fictive temperature concept. The strain hardening can be modeled by a back stress approach represented by rubbery chain models (Boyce et al., 1992; Tomita et al., 1998) . Regardless different constitutive laws, the results show that the initiation of necks depends on the strain softening. A larger amount of strain softening induces a more pronounced necking. The development and propagation of necking depend on the strain hardening. A larger strain hardening intervenes the formation of necks and reestablishes a stable state.

Compared with various works on necking, only limited works have been carried out to characterize and model the shear banding in tensile tests on glassy polymers (Sweeney et al., 2007; Kweon and Benzerga, 2013). Sweeney et al. (2007) adopted the same constitutive model to describe both necking and shear banding. However, in order to allow the shear band nucleation, an off-axis loading or an unrealistic large defect has to be introduced. We notice that shear banding is also observed in polymer solutions, soft glassy materials, metallic glass and alloys (Zhang et al., 2005; Ravindranath et al., 2008; Fielding, 2014; Fu et al., 2012). The research on shear banding in those materials systems can also shed light on understanding the occurrence of the similar phenomena in glassy polymers. For example, constitutive models, such as, the effective temperature model (Hinkle and Falk, 2016), the fluidity

Please cite this article as: R. Zhang et al., Aging-dependent strain localization in amorphous glassy polymers: From necking to shear banding, International Journal of Solids and Structures (2018), https://doi.org/10.1016/j.ijsolstr.2018.03.030

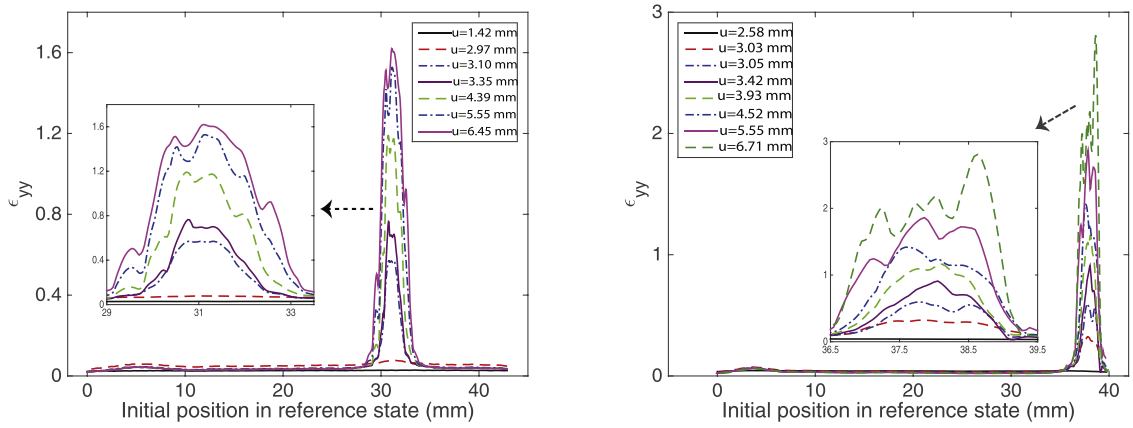

Fig. 10. Section line plots of ϵ_{yy} to show the evolution of the shear bands at stretch rate of a) 0.774 mm/min and b) 7.74 mm/min.

model (Rogers et al., 2008; Moorcroft et al., 2011), the soft glassy rheological model (Fielding, 2014), can all capture the dependence of shear banding on aging. The simulation results suggest that the structural rearrangement plays a central role in formation of shear bands. Though the stress response in the glassy amorphous polymers is several orders of magnitude larger than that of soft glassy materials. The above findings may still help us understand the appearance of shear bands in stiff glassy polymers. In addition, the stability analysis (Jiang and Dai, 2009; Li and Buckley, 2009; Bigoni, 2012) may also be a powerful tool to investigate the onset of the instability.

The temperature increase caused by the plastic dissipation may also contribute to the instability of materials (Bai, 1982; Jiang and Dai, 2009). This is important because competition between self heating, strain softening and strain hardening coexists in polymers. The temperature effect can be significant when the deformation rate is high as shown in Boyce et al. (1992) and Tomita (2000). In this work, the stretch rate varied from 0.774 mm/min to 77.4 mm/min. For the two lower stretch rates, the temperature increase during the deformation process should be insignificant. However, for the highest stretch rate, the heat generation can not be ignored. Thus, infrared camera needs to be used to record the temperature increase of the specimens during deformation. This will be a subject of the future work.

5. Conclusion

Obtaining a fully understanding the deformation localization behaviors in glassy polymers remains a challenging task. In general, three parts of works are needed to address this problem. First, experiments need to be performed to characterize the full field deformation information under various loading conditions. Second, constitutive relationships need to be developed to capture the dependence of the stress response on temperature, rate, aging, and pre-deformation. Third, constitutive models need to be implemented into finite element code to simulate the response of polymers under specific geometry and boundary conditions. The finite element models should be able to reproduce the main experimental observations. Various works (Neale and Tugcu, 1985; Boyce et al., 1992; Wu and van der Giessen, 1994; Govaert et al., 2000; Li and Buckley, 2010) have already been performed to address the above isssues. However, limitations also widely exist. Due to the experimental techniques, previous works were only able to capture the local deformation behaviors and lacked detailed information regarding the initializing and propagating of the localization behaviors. The constitutive models together with the finite element simulation can only describe some specific localization behaviors. A detailed comparison between the experimental observations and simulation results was also not available. The experimental observations in this work can potentially benefit the theoretical and numerical description of localization in glassy polymers.

We used DIC to investigate the influence of physical aging and deformation rate on the tensile deformation behaviors of PETG. The main findings are summarized as follows:

- It was found that the amount of the strain softening increased with deformation rate and physical aging. The quenched polymers exhibited a more smooth strain softening behaviors than the annealed polymers. The quenched polymers were also more ductile than the annealed polymers.
- During the uniaxial tension, homogeneous deformation can only be observed in the pre-yield region. Inhomogeneous deformation occurred when reaching the post-yield strain softening region. The quenched polymers exhibited the localization as necking, while the localization type of the annealed polymers was shear banding.
- After the instability occurred, the localization zones, both necks and shear bands, propagated with the stretch. Most of the deformation occurred in the localization regions. The strain in the other parts of the specimen was negligible.
- Deformation rate also influenced the deformation behaviors. As stretch rate increased, the maximum strain in necks and shear bands increased at the same global displacement. The localization was more severe in shear bands than in necks, which resulted in a smaller failure strain in the annealed conditions.

Though in this work we have successfully applied the DIC technique to study the thermal treatment on the deformation localization behaviors, several limitations still exist and need to be addressed in the future work. First, we used 2D DIC to characterize the deformation. This can not capture the out of plane deformation, which is obvious when shear bands appear. Thus, 3D DIC is needed to fully capture the full field deformation information. Second, specimen geometry has a significant influence on the strain localization. We will perform experiments to investigate this effect. Third, in this work, we show that a transition from necking to shear banding can occur with aging. In order to identify the critical condition for such transition, experiments on polymers with various thermal history have to be performed. At high deformation rate, the inhomogeneous deformation is accompanied by the local temperature increase. A combination of infrared imaging and DIC can reveal different contributions of temperature and nonequilibrium structure to the deformation localization. Currently we are

Please cite this article as: R. Zhang et al., Aging-dependent strain localization in amorphous glassy polymers: From necking to shear banding, International Journal of Solids and Structures (2018), https://doi.org/10.1016/j.ijsolstr.2018.03.030

also developing constitutive models to understand the physical mechanism behind necking and shear banding.

Acknowledgments

This work is supported by the National Natural Science Foundation of China (Grant No. 11502068, 51679078), the Fundamental Research Funds for Central Universities, Hohai University (Grant No. 2016B01414) and China Postdoctoral Science Foundation Funded Project (Grant No. 2017T100322) .

References

Archer, J.S., Lesser, A.J., 2011. Shear band formation and mode ii fracture of polymeric glasses. J. Polym. Sci., Part B 49 (2), 103–114.
Argon, A., 2011. Craze initiation in glassy polymers–revisited. Polymer 52 (10), 2319–2327.
Bai, Y., 1982. Thermo-plastic instability in simple shear. J. Mech. Phys. Solids 30 (4), 195–207.
Bauwens, J.C., 1967. Déformation plastique des hauts polymères vitreux soumis á un système de contraintes quelconque. J. Polym. Sci., Part B 5 (6), 1145–1156.
Bigoni, D., 2012. Nonlinear Solid Mechanics: Bifurcation Theory and Material Instability. Cambridge University Press.
Bowden, P., 1973. The yield behaviour of glassy polymers. In: The physics of glassy polymers. Springer, pp. 279–339.
Boyce, M.C., Montagut, E., Argon, A., 1992. The effects of thermomechanical coupling on the cold drawing process of glassy polymers. Polym. Eng. Sci. 32 (16), 1073–1085.
Brady, T., Yeh, G., 1971. Yielding behavior of glassy amorphous polymers. J. Appl. Phys. 42 (12), 4622–4630.
Cai, Y., Zhang, Q., Yang, S., Fu, S., Wang, Y., 2016. Experimental study on three-dimensional deformation field of portevin–le chatelier effect using digital image correlation. Exp. Mech. 56 (7), 1243–1255.
Chau, C., Li, J., 1979. Some observations of coarse shear bands in polystyrene. J. Mater. Sci. 14 (7), 1593–1608.
Chowdhury, K., Benzerga, A.A., Talreja, R., 2008. A computational framework for analyzing the dynamic response of glassy polymers. Comput. Methods Appl. Mech. Eng. 197 (49), 4485–4502.
Cross, A., Haward, R., 1978. Orientation hardening of pvc. Polymer 19 (6), 677–682.
Dobovšek, I., Polonica, A., 2015. Some aspects of shear yielding and emergence of shear bands in solid polymers. Acta Physica 128 (4), 619–623.
Dooling, P., Buckley, C., Rostami, S., Zahlan, N., 2002. Hot-drawing of poly (methyl methacrylate) and simulation using a glass–rubber constitutive model. Polymer 43 (8), 2451–2465.
Dupaix, R.B., Boyce, M.C., 2005. Finite strain behavior of poly (ethylene terephthalate)(pet) and poly (ethylene terephthalate)-glycol (petg). Polymer 46 (13), 4827–4838.
Engqvist, J., Hall, S., Wallin, M., Ristinmaa, M., Plivelic, T., 2014. Multi-scale measurement of (amorphous) polymer deformation: simultaneous x-ray scattering, digital image correlation and in-situ loading. Exp. Mech. 54 (8), 1373–1383.
Fielding, S.M., 2014. Shear banding in soft glassy materials. Rep. Prog. Phys. 77 (10). 102601
Fu, S., Cheng, T., Zhang, Q., Hu, Q., Cao, P., 2012. Two mechanisms for the normal and inverse behaviors of the critical strain for the portevin–le chatelier effect. Acta Mater. 60 (19), 6650–6656.
Gao, Y., Cheng, T., Su, Y., Xu, X., Zhang, Y., Zhang, Q., 2015. High-efficiency and high--accuracy digital image correlation for three-dimensional measurement. Opt. Lasers Eng. 65, 73–80.
Govaert, L., Timmermans, P., Brekelmans, W., 2000. The influence of intrinsic strain softening on strain localization in polycarbonate: modeling and experimental validation. J. Eng. Mater Technol. 122 (2), 177–185.
Grytten, F., Daiyan, H., Polanco-Loria, M., Dumoulin, S., 2009. Use of digital image correlation to measure large-strain tensile properties of ductile thermoplastics. Polym. Test. 28 (6), 653–660.
Heinz, S.R., Wiggins, J.S., 2010. Uniaxial compression analysis of glassy polymer networks using digital image correlation. Polym. Test. 29 (8), 925–932.
Hinkle, A.R., Falk, M.L., 2016. A small-gap effective-temperature model of transient shear band formation during flow. J. Rheol. 60 (5), 873–882.
Jang, B., Uhlmann, D., Vander Sande, J., 1984. Ductile–brittle transition in polymers. J. Appl. Polym. Sci. 29 (11), 3409–3420.
Jerabek, M., Major, Z., Lang, R., 2010. Strain determination of polymeric materials using digital image correlation. Polym. Test. 29 (3), 407–416.
Jiang, H., Zhang, J., Yang, Z., Jiang, C., Kang, G., 2017. Modeling of competition between shear yielding and crazing in amorphous polymers? scratch. Int. J. Solids Struct. 124, 215–228.
Jiang, M., Dai, L., 2009. On the origin of shear banding instability in metallic glasses. J. Mech. Phys. Solids 57 (8), 1267–1292.
Kattan, M., Dargent, E., Ledru, J., Grenet, J., 2001. Strain-induced crystallization in uniaxially drawn PETG plates. J. Appl. Polym. Sci. 81 (14), 3405–3412.
Kierkels, J., Dona, C.L., Tervoort, T., Govaert, L., 2008. Kinetics of re-embrittlement of (anti) plasticized glassy polymers after mechanical rejuvenation. J. Polym. Sci., Part B 46 (2), 134–147.
Kweon, S., Benzerga, A., 2013. Finite element implementation of a macromolecular viscoplastic polymer model. Int. J. Numer. Methods Eng. 94 (10), 895–919.
Legrand, D., 1969. Crazing, yielding, and fracture of polymers. i. ductile brittle transition in polycarbonate. J. Appl. Polym. Sci. 13 (10), 2129–2147.
Lei, D., Yang, L., Xu, W., Zhang, P., Huang, Z., 2017. Experimental study on alarming of concrete micro-crack initiation based on wavelet packet analysis. Constr. Build. Mater. 149, 716–723.
Li, H., Buckley, C., 2009. Evolution of strain localization in glassy polymers: a numerical study. Int. J. Solids Struct. 46 (7), 1607–1623.
Li, H., Buckley, C., 2010. Necking in glassy polymers: effects of intrinsic anisotropy and structural evolution kinetics in their viscoplastic flow. Int. J. Plast. 26 (12), 1726–1745.
Liu, G., Zhao, D., Zuo, Y., 2015. Modified adam–gibbs models based on free volume concept and their application in the enthalpy relaxation of glassy polystyrene. J. Non Cryst. Solids 417, 52–59.
Meijer, H.E.H., Govaert, L.E., 2005. Mechanical performance of polymer systems: the relation between structure and properties. Prog. Polym. Sci. 30 (8–9), 915–938.
van Melick, H., Govaert, L., Meijer, H., 2003. Localisation phenomena in glassy polymers: influence of thermal and mechanical history. Polymer 44 (12), 3579–3591.
Moorcroft, R.L., Cates, M.E., Fielding, S.M., 2011. Age-dependent transient shear banding in soft glasses. Phys. Rev. Lett. 106 (5). 055502
Murienne, B.J., Chen, M.L., Quigley, H.A., Nguyen, T.D., 2016. The contribution of glycosaminoglycans to the mechanical behaviour of the posterior human sclera. J. R. Soc. Interf. 13 (119). 20160367
Neale, K., Tugcu, P., 1985. Analysis of necking and neck propagation in polymeric materials. J. Mech. Phys. Solids 33 (4), 323–337.
Pan, B., Qian, K., Xie, H., Asundi, A., 2009. Two-dimensional digital image correlation for in-plane displacement and strain measurement: a review. Meas. Sci. Technol. 20 (6). 062001
Pan, B., Yu, L., Wu, D., 2015. Thermo-mechanical response of superalloy honeycomb sandwich panels subjected to non-steady thermal loading. Mater. Des. 88, 528–536.
Pan, B., Yu, L., Yang, Y., Song, W., Guo, L., 2016. Full-field transient 3d deformation measurement of 3d braided composite panels during ballistic impact using single-camera high-speed stereo-digital image correlation. Compos. Struct. 157, 25–32.
Poulain, X., Kohlman, L., Binienda, W., Roberts, G., Goldberg, R., Benzerga, A., 2013. Determination of the intrinsic behavior of polymers using digital image correlation combined with video-monitored testing. Int. J. Solids Struct. 50 (11), 1869–1878.
Ravindranath, S., Wang, S.Q., Olechnowicz, M., Quirk, R.P., 2008. Banding in simple steady shear of entangled polymer solutions. Macromolecules 41 (7), 2663–2670.
Rogers, S.A., Vlassopoulos, D., Callaghan, P., 2008. Aging, yielding, and shear banding in soft colloidal glasses. Phys. Rev. Lett. 100 (12). 128304
Semkiv, M., Hütter, M., 2016. Modeling aging and mechanical rejuvenation of amorphous solids. J. Non-Equilib. Thermodyn. 41 (2), 79–88.
Stoclet, G., Lefebvre, J., Séguéla, R., Vanmansart, C., 2014. In-situ saxs study of the plastic deformation behavior of polylactide upon cold-drawing. Polymer 55 (7), 1817–1828.
Sweeney, J., Caton-Rose, P., Spares, R., Coates, P., 2007. Unified model of necking and shear banding in amorphous and semicrystalline polymers. J. Appl. Polym. Sci. 106 (2), 1095–1105.
Thomas, T., 1953. On the inclination of plastic slip bands in flat bars in tension tests. Proc. Natl. Acad. Sci. 39 (4), 257–265.
Tomita, Y., 2000. Constitutive modelling of deformation behavior of glassy polymers and applications. Int. J. Mech. Sci. 42 (8), 1455–1469.
Tomita, Y., Adachi, T., Sik, P.S., 1997. Computational simulation of three-dimensional neck propagation in polymeric specimens under tension and hybrid identification of constitutive equation. Int. J. Mech. Sci. 39 (8), 913–923.
Tomita, Y., Adachi, T., Tanaka, S., 1998. Computational prediction of instability propagation in glassy polymers. Arch. Comput. Methods Eng. 5 (2), 167–198.
Tung, S.H., Shih, M.H., Kuo, J.C., 2010. Application of digital image correlation for anisotropic plastic deformation during tension testing. Opt. Lasers Eng. 48 (5), 636–641.
Unwin, A., Duckett, R., Ward, I.M., Collins, T., Sweeney, J., Coates, P.D., 2002. Suppression of necking in polyethylene. J. Appl. Polym. Sci. 86 (12), 3135–3147.
Wu, P., van der Giessen, E., 1994. Analysis of shear band propagation in amorphous glassy polymers. Int. J. Solids Struct. 31 (11), 1493–1517.
Wu, P., van der Giessen, E., 1995. On neck propagation in amorphous glassy polymers under plane strain tension. Int. J. Plast. 11 (3), 211–235.
Wu, P., Van der Giessen, E., 1996. Computational aspects of localized deformations in amorphous glassy polymers. Eur. J. Mech.-A/Solids 15 (5), 799–823.
Wu, W., Turner, A., 1973. Shear bands in polycarbonate. J. Polym. Sci., Part B 11 (11), 2199–2208.
Xiao, R., Choi, J., Lakhera, N., Yakacki, C., Frick, C., Nguyen, T., 2013. Modeling the glass transition of amorphous networks for shape-memory behavior. J. Mech. Phys. Solids 61 (7), 1612–1635.
Xiao, R., Ghazaryan, G., Tervoort, T.A., Nguyen, T.D., 2017. Modeling energy storage and structural evolution during finite viscoplastic deformation of glassy polymers. Phys. Rev. E 95 (6). 063001
Xiao, R., Nguyen, T.D., 2015. An effective temperature theory for the nonequilibrium behavior of amorphous polymers. J. Mech. Phys. Solids 82, 62–81.
Xu, W., Wu, F., Jiao, Y., Liu, M., 2017. A general micromechanical framework of effective moduli for the design of nonspherical nano-and micro-particle reinforced composites with interface properties. Mater. Des. 127, 162–172.

Please cite this article as: R. Zhang et al., Aging-dependent strain localization in amorphous glassy polymers: From necking to shear banding, International Journal of Solids and Structures (2018), https://doi.org/10.1016/j.ijsolstr.2018.03.030

Yang, A.M., Wang, R., Lin, J., 1996. Ductile-brittle transition induced by aging in poly (phenylene oxide) thin films. Polymer 37 (25), 5751–5754.
Ye, J., André, S., Farge, L., 2015. Kinematic study of necking in a semi-crystalline polymer through 3d digital image correlation. Int. J. Solids Struct. 59, 58–72.
Yu, J.H., . McWilliams, B.A., Kaste, R.P., 2016. Digital image correlation analysis and numerical simulation of aluminum alloys under quasi-static tension after necking using the bridgman's correction method. Exp. Tech. 40 (5), 1359–1367.
Zhang, Q., Jiang, Z., Jiang, H., Chen, Z., Wu, X., 2005. On the propagation and pulsation of portevin-le chatelier deformation bands: an experimental study with digital speckle pattern metrology. Int. J. Plast. 21 (11), 2150–2173.
Zhu, R., Zhou, J., Jiang, H., Zhang, D., 2012. Evolution of shear banding in fully dense nanocrystalline ni sheet. Mech. Mater. 51, 29–42.

Please cite this article as: R. Zhang et al., Aging-dependent strain localization in amorphous glassy polymers: From necking to shear banding, International Journal of Solids and Structures (2018), https://doi.org/10.1016/j.ijsolstr.2018.03.030